









Lysis Cassette-Mediated Exoprotein Release in *Yersinia entomophaga* Is Controlled by a PhoB-Like Regulator

 Marion Schoof,^a  Maureen O'Callaghan,^a  Charles Hefer,^a  Travis R. Glare,^b  Amber R. Paulson,^c  Mark R. H. Hurst^a

^aAgResearch, Resilient Agriculture, Lincoln Research Centre, Lincoln, New Zealand

^bWine and Molecular Biosciences Dept, Faculty of Agriculture and Life Sciences, Lincoln University, Lincoln, New Zealand

^cBritish Columbia Ministry of Environment and Climate Change Strategy, Victoria, British Columbia, Canada

ABSTRACT Secretion of exoproteins is a key component of bacterial virulence, and is tightly regulated in response to environmental stimuli and host-dependent signals. The entomopathogenic bacterium *Yersinia entomophaga* MH96 produces a wide range of exoproteins including its main virulence factor, the 2.46 MDa insecticidal Yen-Tc toxin complex. Previously, a high-throughput transposon-based screening assay identified the region of exoprotein release (YeRER) as essential to exoprotein release in MH96. This study defines the role of the YeRER associated ambiguous holin/endolysin-based lysis cluster (ALC) and the novel RoeA regulator in the regulation and release of exoproteins in MH96. A mutation in the ambiguous lysis cassette (ALC) region abolished exoprotein release and caused cell elongation, a phenotype able to be restored through *trans*-complementation with an intact ALC region. Endogenous ALC did not impact cell growth of the wild type, while artificial expression of an optimized ALC caused cell lysis. Using HolA-sfGFP and Rz1-sfGFP reporters, Rz1 expression was observed in all cells while HolA expression was limited to a small proportion of cells, which increased over time. Transcriptomic assessments found expression of the genes encoding the prominent exoproteins, including the Yen-Tc, was reduced in the *roeA* mutant and identified a 220 ncRNA of the YeRER intergenic region that, when *trans* complemented in the wildtype, abolished exoprotein release. A model for *Y. entomophaga* mediated exoprotein regulation and release is proposed.

IMPORTANCE While theoretical models exist, there is not yet any empirical data that links ALC phage-like lysis cassettes with the release of large macro-molecular toxin complexes, such as Yen-Tc in Gram-negative bacteria. In this study, we demonstrate that the novel *Y. entomophaga* RoeA activates the production of exoproteins (including Yen-Tc) and the ALC at the transcriptional level. The translation of the ALC holin is confined to a subpopulation of cells that then lyse over time, indicative of a complex hierarchical regulatory network. The presence of an orthologous RoeA and a HolA like holin 5' of an eCIS Afp element in *Pseudomonas chlororaphis*, combined with the presented data, suggests a shared mechanism is required for the release of some large macromolecular protein assemblies, such as the Yen-Tc, and further supports classification of phage-like lysis clusters as type 10 secretion systems.

KEYWORDS transcriptional regulator, transcriptomics, holin, secretion, entomopathogen, toxin complex, protein secretion

The release of exoproteins from bacteria plays a role in their nutrient acquisition, antimicrobial resistance, and delivery of toxins or other virulence factors enabling pathogenic bacteria to attach to and/or invade host tissues (1–3). To release exoproteins, several secretion pathways have evolved to transport proteolytic enzymes and other virulence factors across the protective lipid bilayer of the Gram-negative bacterial cell wall. These pathways range from simple protein channels and pores that span the

Editor John M. Attack, Griffith University

Copyright © 2023 Schoof et al. This is an open-access article distributed under the terms of the [Creative Commons Attribution 4.0 International license](https://creativecommons.org/licenses/by/4.0/).

Address correspondence to Marion Schoof, marion.schoof@agresearch.co.nz, or Mark R. H. Hurst, mark.hurst@agresearch.co.nz.

The authors declare no conflict of interest.

Received 26 January 2023

Accepted 27 February 2023

Published 23 March 2023

cell wall to more complex multicomponent secretion systems, including the Type 1–9 secretion systems (T1-9SS) (4, 5).

In addition to cell wall-based secretion systems, indirect mechanisms, such as the release of membrane vesicles and cell lysis via phage-like lysis cassettes (6–8), have been recognized as alternative mechanisms for protein release and/or transport (9–11). Palmer et al. (2021) modeled a T10SS on the *Serratia marcescens* ChiWXYZ-chitinase secretion pathway, where the nonspecific holin pore ChiW allows translocation of proteins, including the hydrolase ChiX, which degrades peptidoglycan in the cell wall (12). The ChiWXYZ can be described as a phage-derived lysis cassette which, upon activation, causes the host cell to lyse (13).

The broad host range entomopathogen *Yersinia entomophaga* strain MH96 encodes multiple virulence factors including adhesins, Type 3 and Type 6 secretion systems, proteolytic enzymes, and insecticidal toxins (14). Many of these virulence genes are up-regulated during haemocoelic infection of *Galleria mellonella* at 25°C (15). In Luria Bertani (LB) broth at temperatures of $\leq 25^\circ\text{C}$ *Y. entomophaga* releases large quantities of exoprotein, including the Yen-Tc (16). The production of exoprotein is elevated through exponential growth and decreases through stationary phase (17). Based on reduced exoprotein in LB broth at 37°C, the production of these exoproteins, including the Yen-Tc, is likely under the control of a temperature sensor (16, 18).

Through use of a high-throughput secretion assay (HESA), a gene cluster termed *Y. entomophaga* region of exoproteome release (YeRER) was identified, which controls exoproteome production (including the Yen-Tc) by this species (17). The YeRER comprises a predicted phage-like lysis cassette designated the ambiguous holin/endolysin-based lysis cluster (ALC) - encoded by *holA*, *pepB*, *rz*, and *rz1*- and a predicted DNA binding regulator (RoeA) separated by a 1086 bp intergenic region. The HESA identified 3 transposon insertions (H45, H4, and H31) respectively located 70, 120, and 237 nucleotides 5' of the ALC *holA* initiation codon, respectively, and 1 transposon mutant (H12) with a single transposon insertion within *roeA*, which significantly reduced exoprotein production. Further to this, a 3-bp deletion in a spontaneous exoprotein deficient mutant strain K18 was identified in the YeRER intergenic region 131 bp 5' of the *roeA* initiation codon (17). Based on these findings, it is likely that RoeA is a global activator of MH96 exoprotein production via control of the lysis cassette.

In silico analysis of the 15 kDa RoeA protein identified the protein to be of the PhoB family of two-component regulators (TCR) (19, 20). In this context, PhoB-like proteins comprise a membrane-bound histidine kinase domain that responds to specific environmental stimuli, and a receiver domain which acts as a transcriptional regulator upon its phosphorylation by its cognate histidine kinase (21–24).

To date, the *Yersinia enterocolitica* W22703 thermoregulatory mechanism involving the LysR type regulators *tcaR1* and *tcaR2* located 5' of the W22703-encoded *tc* genes, and the Tc-PAI_{ye} lysis cassette juxtaposed to *TcaC* and *TccC* are the most studied example of regulation and Tc release (25, 26). In this system, it has been proposed the lysis cassette, comprised of *holY*, *elyY*, *yRz*, and *rRz1*, can cause cell lysis, but no biological proof of the function has yet been demonstrated.

Based on the unique properties of RoeA, its associated ALC lysis cassette and its role in exoprotein production, we have used a combination of fluorescent and enzymatic reporter genes, microscopy, and transcriptomics to determine the mechanism by which the MH96 lysis cassette-mediated exoprotein release is regulated.

RESULTS

Exoprotein release by the ambiguous lysis cluster (ALC) of the YeRER. Using gene synteny studies, orthologs of the MH96-phage- λ -like lysis cassette, typified by the presence of a holin, a peptidase, and 1 to 2 spanin proteins, were identified co-located within a toxin complex (Tc) of the *Yersinia* genus (Fig. 1A). In contrast to phage λ lysis cassettes, the holin (HolA) of the MH96 ALC and other *Yersinia* strains do not contain a dual-start motif, forming the holin (S105)- antiholin (S107) complex (27, 28),

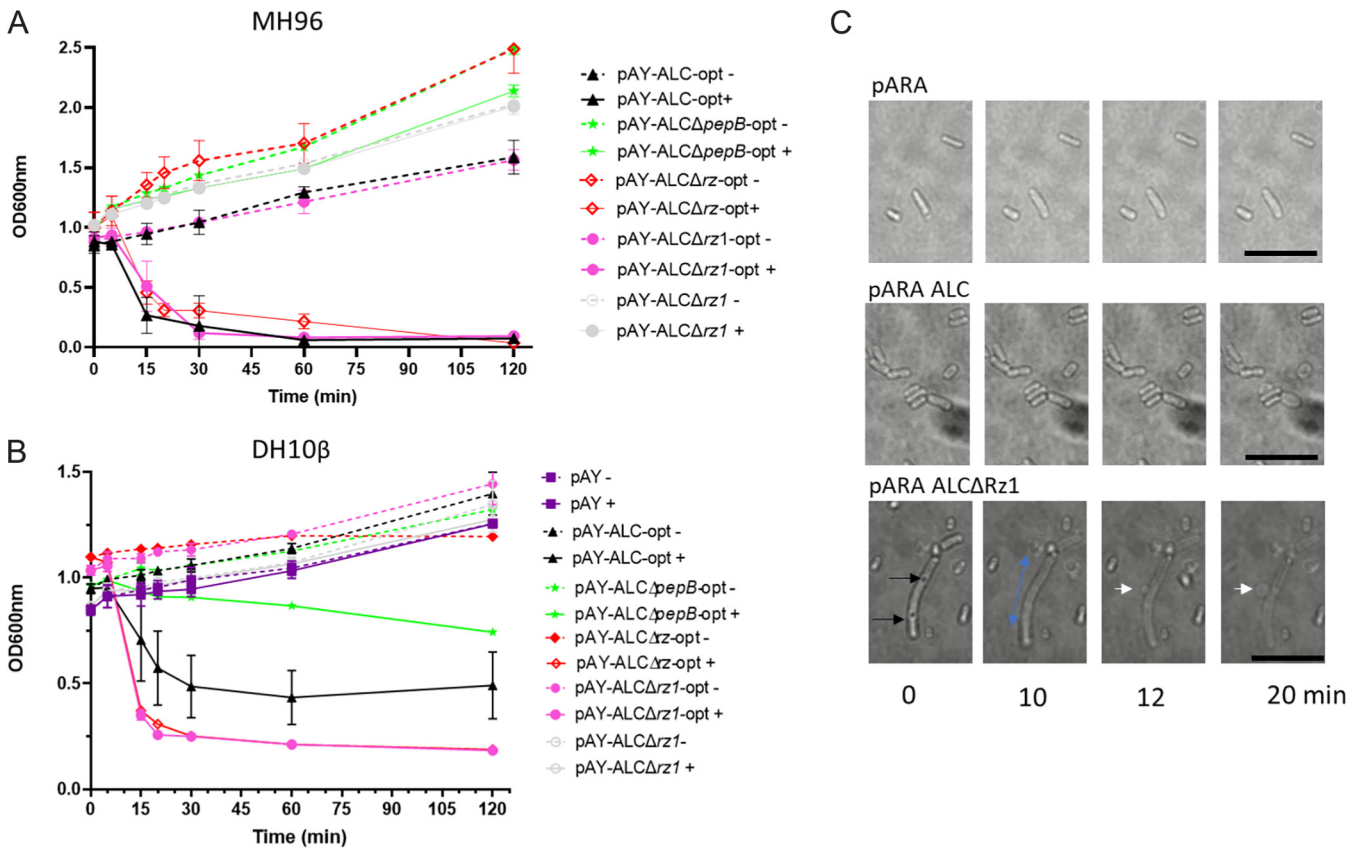


FIG 2 OD₆₀₀ assessment of lysis activity of the pAY-ALC constructs induced with 0.02% arabinose (+) compared to uninduced culture (-) over 20 min. (A) Lysis activity of ALC expressed in MH96. (B) Lysis activity of ALC expressed in *E. coli*. (C) Live-cell imaging of cells upon induction with 0.6% arabinose, over 20 min. Black arrows denote localized dark areas, blue arrows denote directional cell elongation, white arrows denote membrane blebbing. Scale bar, 10 μm.

as identified by SDS-PAGE and electrospray ionization ion trap-tandem mass spectrometry (LC-ESI-MS/MS) (Fig. 1B and Fig. S4).

The deletion of the ALC in ΔALC (Table S1) did not alter cell viability as determined through CFU counts and LIVE/DEAD stain (Fig. S5), indicating that the ALC may not cause cell lysis or, alternatively, that ALC-mediated cell lysis and death is compensated for by growth of the non-lysed cell population and is therefore not detectable through CFU counts.

Induction of the arabinose inducible vector pAY-ALCΔrz1 (Table S2) harboring the ALC with its native gene arrangement of *hola*, *pepB*, and *rz* but devoid of *rz1* resulted in no change in optical cell density (OD₆₀₀) in either MH96 (Fig. 2A) or *Escherichia coli* DH10B (Fig. 2B). This likely reflects the requirement for back-translational coupling (termination-reinitiation), which is typical for λ phage-like lysis (29, 30). However, the use of the uncoupled ALC-encoding ORF in the pAY-ALC-opt vector series (Table S3) resulted in rapid cell lysis and a concurrent decrease of OD₆₀₀ from 1 to 0.2 within 15 min post induction (mpi) (Fig. 2C and Movie S1). Live-cell imaging of pAY-ALCΔRz1-opt revealed cell elongation with brightening at cell poles; some elongated cells showed 1 to 3 small localized dark areas, which disappeared within 15 min (Fig. 2C and Movie S2). Prior to cell lysis (20 mpi) localized bulging of cells leading to membrane blebbing (15 mpi) was observed (Fig. 2C and Movie S2). In MH96, the expression of the ALC missing either i-spanin Rz or o-spanin Rz1 in pAY-ALCΔrz-opt and pAY-ALCΔrz1-opt caused rapid cell lysis as seen in ALC-opt expression (Fig. 2A). However, lysis activity of the ALC-opt in *E. coli* increased in the absence of either spanin (Fig. 2B), which may reflect cell wall composition differences between these species. In the absence of *pepB*, slow cell lysis was observed when inducing pAY-ALCΔpepB-opt in *E. coli* (Fig. 2B).

To correlate ALC activity with MH96 cell lysis, the translational *HolA*-sfGFP and *Rz1*-

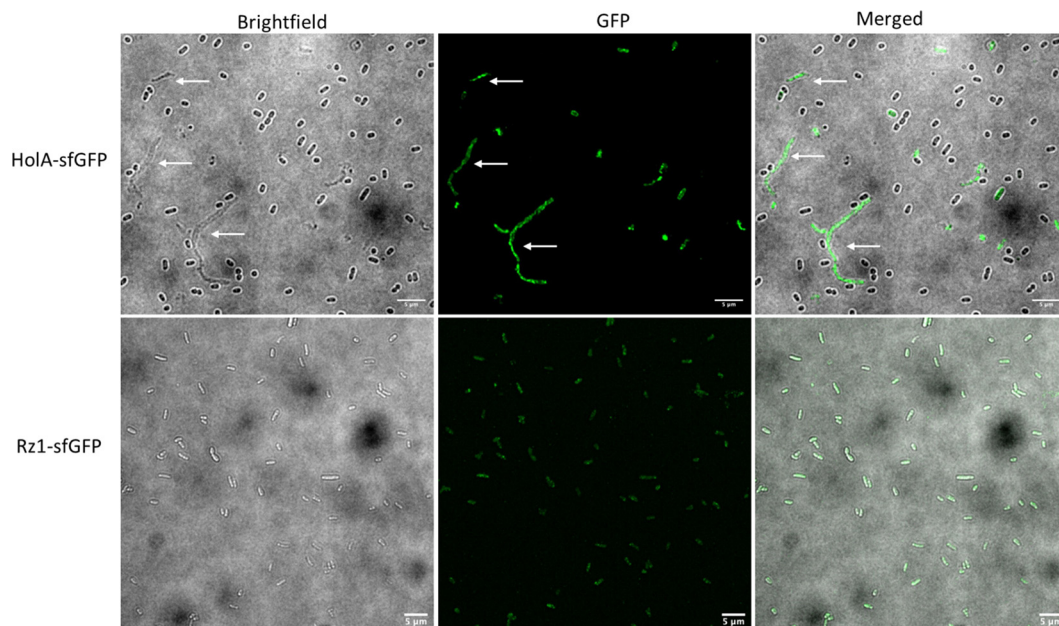


FIG 3 Light and fluorescence microscopy of MH96 cells expressing HoIA-sfGFP and Rz1-sfGFP. Brightfield, GFP and Merged images shown. White arrows denote elongated cells. Scale bar, 5 μ m.

sfGFP constructs were assessed in LB broth cultures at 25°C. During early exponential growth (6 to 8 h), 15% of HoIA-sfGFP cells were fluorescing, increasing to 44% at mid-late exponential phase (10 to 12 h postinoculation [hpi]) and decreasing slightly to 41% at stationary phase (>12 hpi). The HoIA-sfGFP signal was observed over the entire cell membrane (Fig. 3) and in elongated cells through these growth phases. Parallel assessments of Rz1-sfGFP found that all stationary phase cells were fluorescing with the entire cell membrane fluorescent (Fig. 3).

The PhoB-like regulator *RoeA* alters ALC, exoprotein, and global gene expression.

Through amino acid alignments and correlation of *RoeA* to the resolved structures of the TCRs, CadC (31), OmpR (20, 32), and PhoB (33), *RoeA* shares a PhoB-like helix-turn-helix (HTH) motif, comprising 3 α -helices, of which α 2 and α 3 are connected by a DNA loop forming the DNA binding structure (33, 34), in which the DNA binding motif resides (Fig. 4). Of interest, the C termini of *RoeA* and *RoeA*-like proteins extend up to 40 amino acids compared to PhoB-like proteins, with the exception of CadC, which harbors a N-terminal HTH motif. Unlike PhoB, *RoeA* has no cognate phosphorylation domain.

Assessing the non-redundant National Center for Biotechnology Information's (nrNCBI) protein database, *RoeA* orthologues were identified in a limited number of bacteria, mainly within Yersiniaceae (sharing 30 to 100% amino acid identity) and Enterobacteriaceae (<30% amino acid identity) (Fig. S3). Of note, a *RoeA* orthologue (40% amino acid similarity to *RoeA*) is located 5' of the Afp/PVC-like eCIS protein complexes of *Pseudomonas chlororaphis*, and is in juxtaposition to a ALC HoIA ortholog (Fig. 1A). Interestingly, a second MH96 *RoeA*-homolog Yen7 is located 5' of Yen-Tc, which is a similar position to the LysR-like regulator *tcaR* of other Tc-encoding *Yersinia* strains (12, 25).

Attempts to delete *roeA* in its entirety were unsuccessful, while SDS-PAGE assessment of MH96 Δ *roeA151::Spec* containing a spectinomycin cassette 151 bp 3' of the *roeA* initiation codon (Table S1) showed an exoproteome profile similar to MH96 (data not shown). This contrasts to the highly reduced exoprotein profile of the transposon insertion H12. Through the positioning of these mutations on the *RoeA* amino acid sequence (Fig. 4), the H12 insertion prevents translation of the entire *RoeA* HTH-motif, while the MH96 Δ *roeA151::Spec* insertion retained 90% of the α 2 helix and a partial HTH motif, which may enable its functionality. Based on the different exoproteome profile of H12 and MH96 Δ *roeA151::Spec* the genome of H12 was sequenced from

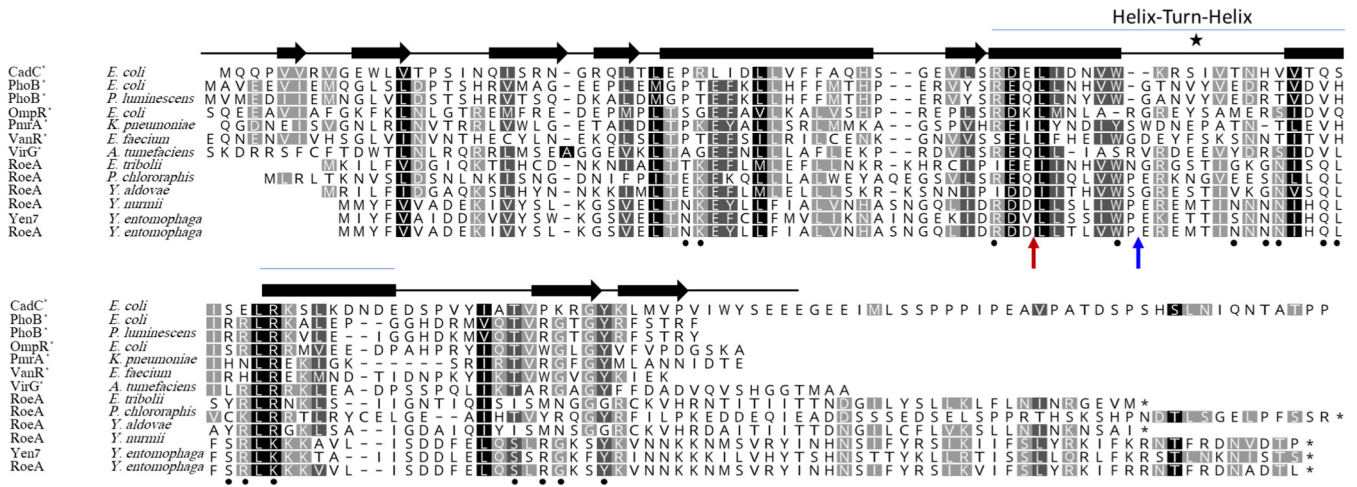


FIG 4 Amino acid alignment and secondary structure prediction of RoeA and its Yen7 orthologue and selected PhoB type regulators. Black filled circles denote PhoB residues linked to DNA binding (33), and area marked by a star denotes HTH-motif (34). Red and blue arrows denote respective MH96ΔroeA151::Spec and H12 mutation sites.

where a single transposon insertion within *roeA* was validated and the H12 *roeA*- strain was used in subsequent assessments.

To further define the role of RoeA in the transcriptional regulation of exoproteins and their release mechanism, the *roeA* H12 mutant and the wild type MH96 were subjected to transcriptomic assessments, targeting early stationary growth phase at approximately 9.6 log₁₀ CFU mL⁻¹. Through DEseq2 analysis of the transcriptome, the H12 *roeA* mutant resulted in the differential expression of 2235 (53%) genes relative to MH96. For analysis purposes we concentrated on genes with transcription levels increased or decreased by log₂ fold >|1|, and identified 406 genes that were significantly overexpressed and 500 that were significantly downregulated (Fig. 5).

While most differentially regulated genes in *roeA* mutants have no assigned COG-classification, the H12 *roeA* mutation affected genes with a wide range of functions, with greater effects on genes involved in: (i) post-translational modification, such as heat shock proteins, DnaJK and GroEL molecular chaperones; (ii) translation, such as ribosomal proteins; and (iii) intracellular trafficking and secretion, such as genes of the T2SS (File S1). Other genes function in energy production, and carbohydrate, amino acid and inorganic ion transport, and metabolism (File S1). Importantly, the transcription of genes encoding for the ALC, its associated *roeA*, Yen-Tc, the *roeA* homologue *yen7*, and the genes encoding the predominant wildtype MH96 exoproteins PL78_18785, PL78_05495, PL78_11910, and PL78_05310 (validated through LC-ESI-MS/MS) were significantly reduced in the *roeA* H12 mutant (File S1).

Temperature dependent regulation of RoeA and its effect on exoprotein production. Based on the role of RoeA in the transcription of exoproteins including the Yen-Tc and the effect of temperature on virulence regulation *in vitro* (35) and *in vivo* in *G. mellonella* at 25°C and 37°C (15), we investigated the effect of temperature on the translation of RoeA and the Yen-Tc associated Chi1, as an exoprotein proxy.

Using a P_{roeA}::*lacZ* cis-merodiploid strain cultured at 25°C in LB broth, the β-galactosidase (β-gal) levels increased during exponential growth phase but stabilized at stationary growth phase (Fig. 6), which correlates with the increased exoprotein levels produced through the exponential growth phase (17). In parallel assessments, at 37°C P_{roeA}::*lacZ* and P_{chi1}::*lacZ* β-gal levels were significantly reduced compared to 25°C (Fig. 6).

The YeRER intergenic region affects the regulation of the ALC and RoeA. As previously demonstrated in the HESA, 3 mutations (H4, H31, and H45, 5' of the ACL) and the spontaneous K18 mutation (5' *roeA*) were identified in the YeRER intergenic region (17), suggesting an important role for the intergenic region in ALC regulation, and,

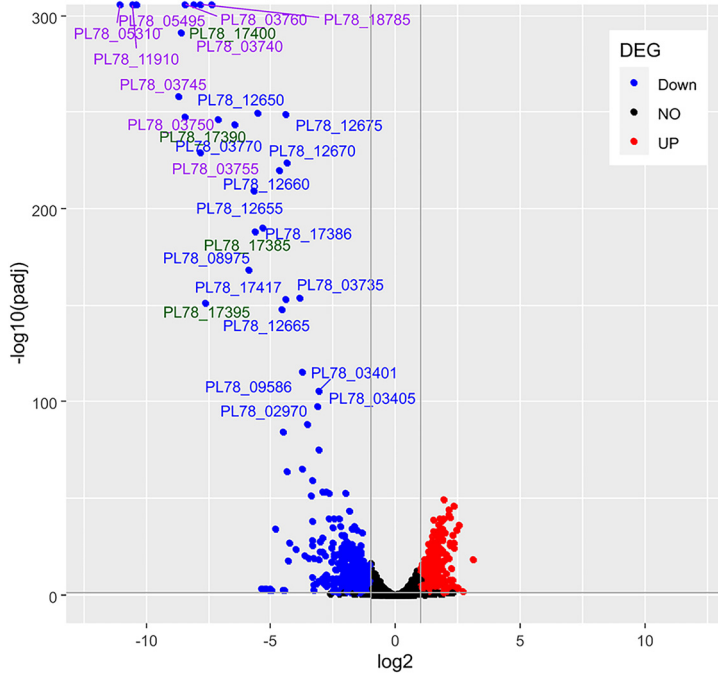


FIG 5 DeSeq2 analysis of gene expression levels of genes that are significantly regulated with $p_{\text{adjust}} < 0.005$ in the *roeA* mutant H12 compared to MH96. Data is depicted as volcano plot with downregulated genes in H12 by a fold change of $\log_2 < -2$ (blue), and upregulated genes by a fold change of $\log_2 > 2$ (red). Genes expressing exoproteins are marked in purple, and YeRER associated genes are marked in green. Genes with fold change \log_2 between -2 and 2 are indicated in black.

therefore, exoprotein release. Through transcriptome assessments, the predicted transcriptional start site of *roeA* and *holA* was located 3 bp and 350 bp 5' of the respective gene (Fig. S6A).

A salient finding through the assessments of the RNAseq mRNA reads was the identification of a low number of mRNA reads spanning a 220 bp region of the YeRER intergenic region in both WT MH96 and the *roeA*- H12 mutant, and the predicted ncRNA designated ncALC220 (Fig. S6A). Based on this information we further interrogated the YeRER nucleotide sequence for potential regulatory signatures (Fig. S6B). The YeRER intergenic region is AT rich with 33.7% G+C relative to 48.6% G+C of the MH96 genome, and harbors several protein binding motifs including those for PhoB and Fur-like proteins, identified using the Prodoric software (Table S4). The *Vibrio cholerae* cyclic AMP receptor protein (CRP) DNA binding motif was found in the core sequence of the degenerate repeats (Fig. S6B). Further investigation of the nucleotide sequences 5' of *roeA*

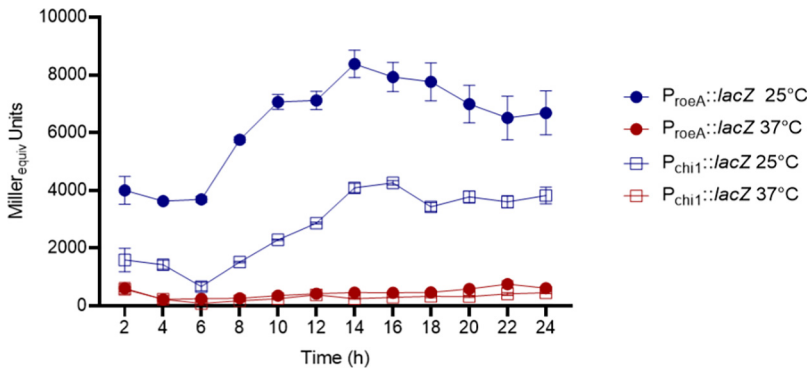


FIG 6 β -galactosidase production of MH96 *cis*-merodiploid $P_{\text{chi1}}::\text{lacZ}$ and $P_{\text{roeA}}::\text{lacZ}$ strains at 25°C and 37°C over a 4 to 24 h duration. Error bars represent \pm SD of biological duplicates and technical replicates from the same culture flask.

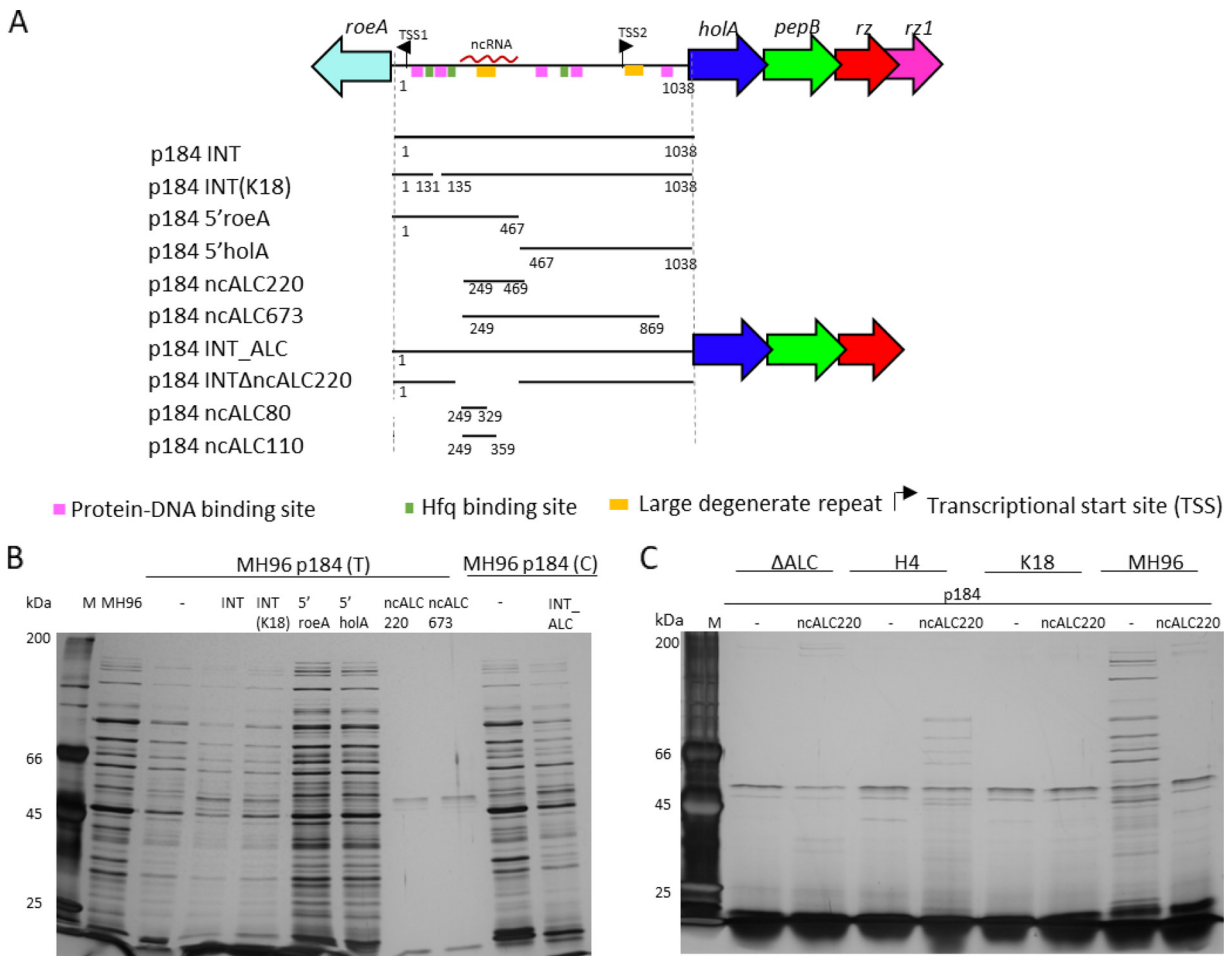


FIG 7 *Trans* complementation of the YeRER intergenic region and the impact in exoprotein release. (A) Schematic of the YeRER, including putative secondary structures and transcription factor binding sites. Depicted are the *trans* complementation vector series p184 p184INT, p184 INT(K18), p184 5'roeA, p1845'holA, p184ncALC220, p184ncALC673, p184INT_ALC, p184INTΔncALC220, p184ncALC80, and p184ncALC110 used for *trans* complementation. (B) SDS-PAGE (10%) of the exoproteome profiles from culture supernatant of MH96 *trans* complemented with the p184 vector series each grown in the presence of 10 μg/mL tetracycline (T) (p184 [T]), empty vector (p184 -), and p184INT_ALC grown in the presence of 30 μg/mL chloramphenicol (C) (p184 [C]). (C) SDS-PAGE (10%) of the exoproteome profiles from supernatant of MH96, K18, H4, and ΔALC containing empty vector pACYC184 (p184 -) or pACYC184 containing the ncALC220 (p184 ncALC220), each grown in the presence of 10 μg/mL tetracycline.

and the *roeA* homologue *yen7*, identified the same H-NS binding site (36) 32 bp 5' of their respective initiation codons (Fig. S6C). Additionally, Hfq binding motifs (5 AATAATA-3') (34) can be found in the intergenic region, including one in the ncALC220 (Fig. S6B).

Based on the bioinformatic analysis of the YeRER associated intergenic region and the potential role of ncALC220 in YeRER regulation, a series of pACYC184 (p184) based vectors (Fig. 7A and Table S2) were constructed enabling their effect on exoprotein production in either a MH96, ΔALC, H4, or K18 background to be determined. The vectors comprise various sections of the intergenic region, ncALC220, and the intergenic region where the ncALC220 sequence was deleted (p184INTΔncALC220) (Fig. 7).

Through assessments by SDS-PAGE, the *trans* complementation with either p184INT or p184ncALC220 in MH96, resulted in reduced exoprotein relative to the vector only MH96 control (Fig. 7B). Importantly the same intergenic region devoid of the 220 bp ncRNA (p184INTΔncALC220) did not alter the MH96 exoprotein profile (Fig. S7A). Truncated versions of ncALC220, namely, ncALC80 (1-80 bp of ncRNA220), and ncALC110 (1-110 bp of ncRNA220), did not alter exoprotein production or cell morphology when *trans* complemented in MH96 (Fig. S7A). The *trans* complementation of p184ncALC220 with either ΔALC or K18 did not restore exoprotein production (Fig. 7C), however a partial

restoration was observed in H4 (transposon insertion 5' of the ALC). Importantly, *trans* complementation with p184INT_ALC in either Δ ALC and H4 resulted in partial restoration of exoprotein but not the Yen-Tc (Fig. S7B, C), and cell morphology with cells of similar size to MH96 (Fig. S3). While *trans* complementation of Δ ALC with either p184INT, p184 5'*holA*, and to a lesser extent with p184INT(K18) or p184ncALC220, resulted in cells of a similar length as observed for MH96 (Fig. S3). Further to this, *trans* complementation with the intergenic region, in full or in part, including the ncRNA220, did not significantly alter cell morphology in H4 being similar in appearance to vector only control (Fig. S3). In K18, none of the *trans* complementation p184 vectors altered either the observed exoprotein (Fig. S7D) or cell morphology (Fig. S3).

To determine if cell elongation observed in H4 and Δ ALC and cell shortening observed in K18 reflects an accumulation/absence of pre-exoprotein within the cell, the culture ($\sim \log_{10}$ 9.6 CFU/mL) cell pellets and supernatant of MH96, K18, H4, and Δ ALC were assessed by SDS-PAGE (Fig. 1B). Pre-exoproteins corresponding to the Yen-Tc (as proxy for exoproteins) were seen in the H4, Δ ALC and MH96 but were absent in K18 and the *roeA* H12 mutant (Fig. 1B). To further define the role of RoeA in exoprotein release, the vector pAY-RoeA was induced in the *roeA* K18 mutant where, with the exception of the Yen-Tc, exoprotein was released (Fig. S7D).

DISCUSSION

The presented data supports the role of the YeRER associated RoeA regulator and the ALC in production of exoprotein by *Y. entomophaga*—a model which is presented in Fig. 8. Differing from MH96, SDS-PAGE assessments of supernatant of the *roeA* mutants H12 and K18, and the ALC mutants Δ ALC and H4 revealed an absence of exoprotein (Fig. 1B) and changes in cell morphology (Fig. S3). The altered phenotype of reduced exoprotein release and changes in cell morphology in H4 and Δ ALC could be restored by *trans* complementation of p184INT_ALC, revealing that its putative RoeA regulator can act in *trans*. The presence of pre-exoprotein precursors, such as the Yen-Tc in the cell pellet of Δ ALC and H4, but no exoprotein (Fig. 1B) supports the mechanistic role of the ALC in exoprotein release. Under the same conditions no pre-exoprotein was observed in the cell pellets of either the H12 *roeA* mutant or K18 (Fig. 1B), further validating the regulatory role of RoeA in the induction of pre-exoprotein including the Yen-Tc.

The induction of the native ALC cassette pAY-ALC Δ *rz1* devoid of the second *rz1* spanin did not cause cell lysis. In *Y. enterocolitica* W22703 induction of its lysis cassette deficient in spanins caused cell lysis (37). For W22703, *holA* and *pepB* are adjacent genes while in MH96 *holA* and *pepB* are overlapping genes on different reading frames. Through uncoupling the ALC system, the induction of pAY-ALC-opt, pAY-ALC Δ *rz1*-opt (devoid of Rz spanin), and pAY-ALC Δ *rz1*-opt (devoid of the Rz1 spanin) caused rapid cell lysis in MH96, indicating the necessity of holin and endopeptidase for lysis. Similar effects were also noted on the induction of these constructs in *E. coli*. Of interest, although the induction pAY-ALC Δ *pepB*-opt devoid of *pepB* had no effect on MH96, its induction in *E. coli* resulted in a low level of cell lysis (Fig. 2B). This may reflect the non-specific pore of the holin allowing other peptidoglycan degrading enzymes to enter the periplasmic space in *E. coli* (38, 39) (Fig. 8).

Fluorescent microscopy of the HolA-sfGFP fusion found fluorescence was confined to a subset of cells of various sizes, wherein the fluorescence was observed throughout the cell. This may reflect the integration of HolA in the inner membrane and subsequent formation of the holin holomer required for release of the endopeptidase as documented in *E. coli* phage λ system and the mycobacteriophage D29 system expressed in *E. coli* prior to cell lysis (40, 41). In contrast, the fluorescence of the spanin Rz1-sfGFP was observed throughout the population and across the entire cell, which was also demonstrated in the spanin complex of the phage λ using a GFP Φ Rz fusion by Berry et al. (2012) (42). The post-transcriptional regulation of ALC is likely through the need for back-translational coupling to uncouple the *holA* and *pepB* ORFs, the process of which was confined to a subset of cells as evidenced using the HolA-sfGFP

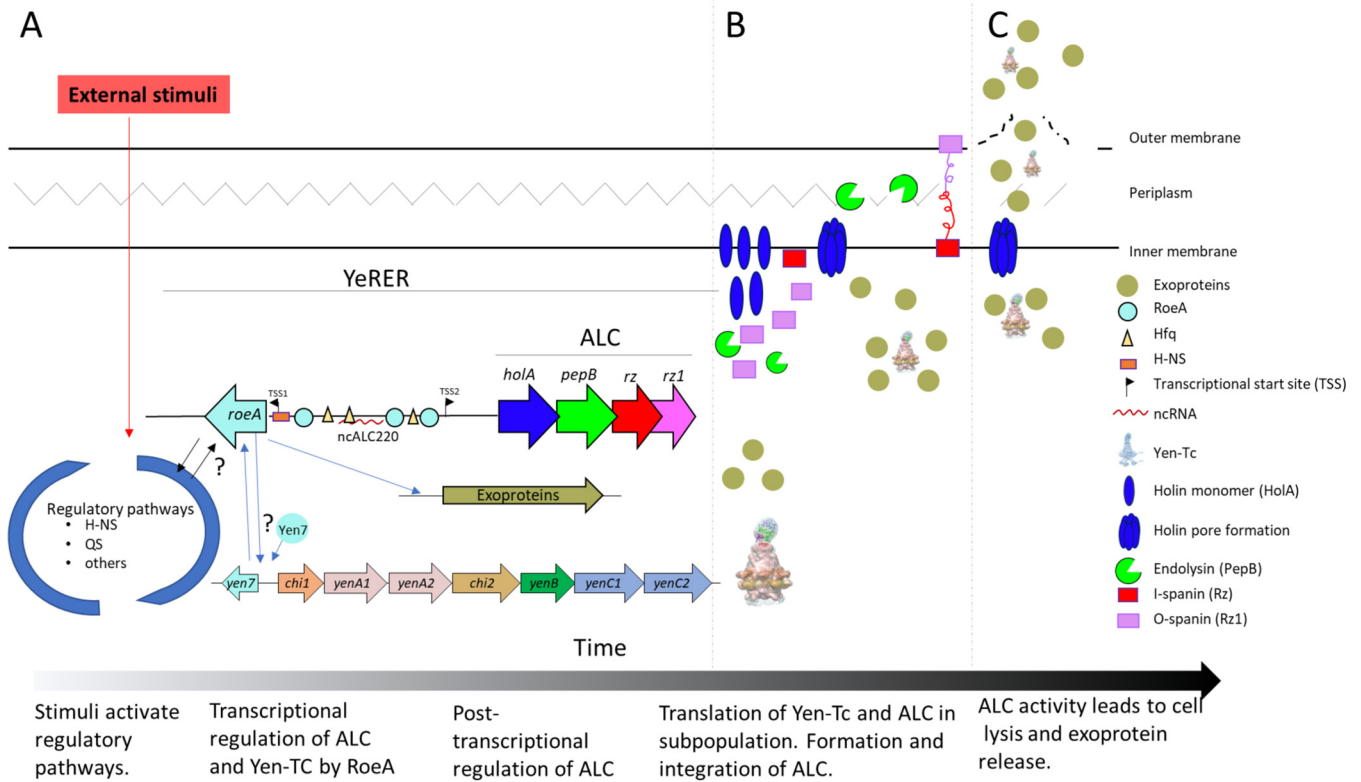


FIG 8 Schematic of the proposed model of *Y. entomophaga* exoprotein release. (A) Devoid of a sensor domain, RoeA is likely activated as part of a larger regulatory system responding to environmental stimuli, such as temperature or stress response. The presence of an H-NS binding consensus sequence at similar nucleotide distances from *roeA* and its *yen7* orthologue suggests that H-NS regulates the expression of these genes. The RoeA-DNA binding motif enables its binding to PhoB-like DNA binding sites in the genome, including within the YeRER intergenic region. RoeA then activates the transcriptional expression of the ALC and exoproteins, including the Yen-Tc, as evidenced through their reduced transcription and the absence of pre-exoprotein in the H18 and H12 *roeA*- cell pellet. The ability of the ncALC220 to reduce exoprotein release when placed in *trans* in MH96 supports the hypothesis that the YeRER intergenic region may interact with mRNA or proteins e.g., Hfq, wherein Hfq binding sites reside within the YeRER intergenic region and within the ncALC220. (B) The ALC is tightly regulated at post-transcriptional level by the termination-reinitiation complex of the ALC operon, as well as yet to be determined post-transcriptional factors linked to ncALC220. Based on its observed expression in a subset of cells, HolA is under tight post-translational regulation. Prior to holin pore formation, exoproteins accumulate in the cell causing cell elongation. Upon holin pore formation, the endolysin PepB and the spanin holin complex enter the periplasm, which subsequently (C) causes cell lysis allowing the release of the exoproteins including the Yen-Tc. Due to inactivation of the ALC, no cell lysis occurs, which inhibits the release of proteins and leads to accumulation of exoproteins in the cell, as observed by SDS-PAGE of the H4 and Δ ALC cell pellets and supernatants, which then causes cell elongation. In the H12 *roeA* mutant, neither the ALC nor exoproteins are produced resulting in uniform sized cells, which do not elongate.

reporter. Similar to phage systems, such as the λ phage, the translation of HolA is likely a rate limiting step of cell lysis (43).

Through RNAseq, the expression 2235 genes including those encoding components of the ALC cluster were significantly reduced in the H12 *roeA* mutant. This included the reduced transcription of several key exoproteins (PL78_18785, PL78_05495, PL78_11910, PL78_05310 [as validated through LC-ESI-MS/MS of wild type MH96 culture supernatant]) and the Yen-Tc. In addition, through the use of $P_{roeA}::lacZ$ and the Yen-Tc $P_{chi1}::lacZ$ reporters, the β -gal activities of both strains proportionally increased through exponential growth in LB broth at 25°C, and were both significantly reduced at 37°C, linking the translation of both RoeA and the Yen-Tc.

Based on the high similarity of RoeA to PhoB and PhoB-like regulators, such as CadC and OmpR (Fig. 4), it is plausible that altered expression of many genes of the H12 *roeA* mutant may reflect the ability of RoeA to bind other yet to be determined genomic sites. Other genes significantly reduced in expression in the H12 *roeA* mutant included ribosomal genes, and genes involved in metabolism. Based on the absence of a ribosomal depletion step in our methodology (refer to materials and methods), these transcriptional changes may cause the cells to enter a state of reduced metabolic activity. The reduced metabolism in H12 and K18 may account for the observed homogenous, mid

-exponential cell culture comprising cells of a shorter length relative to the heterogenous population with a small number of elongated cells observed in wildtype MH96 (Fig. S3). In contrast, a high number of atypically elongated cells were observed in the Δ ALC mutant (Fig. S3).

Interrogation of the *roeA/hoIA* intergenic nucleotide sequence revealed the presence of several nucleotide repeats, PhoB- and H-NS binding motifs, and secondary structures (Fig. S6B and C, and Table S4). The prevalence of a range of different DNA binding motifs and the ncALC220 suggests that the YeRER intergenic region is the substrate for a complex of transcriptional, translational, and post-translational regulation (44) (Fig. S6B and Table S4). The positioning of a H-NS binding consensus sequence at similar nucleotide distances from *roeA* and its *yen7* homologue (Fig. S6C and Table S4) suggests that RoeA is likely under the control of the H-NS regulatory cascade, from where RoeA in turn acts on exoprotein and the ALC expression (Fig. 8). This, in part, parallels the thermoregulation of the *Y. enterocolitica* W22703 LysR-like transcriptional regulator TcaR1/2 and H-NS (25, 26). Of interest, H-NS, a global transcriptional regulator, reacts to environmental cues (45, 46), and may indirectly take the place of a TCR response sensor that is absent in RoeA. Similar H-NS regulatory cascades have been described for H-NS in acid stress resistance in *E. coli* (45, 47). Adding to this, Schoof et al. (16) found transposon mutants H23 and H45 for quorum sensing (QS) N-acyl-homoserine lactone synthetase resulted in reduced exoprotein through the exponential growth phase (17), indicating growth phase dependent regulation of RoeA resulting in exoprotein expressions.

A salient finding was the ability of the intergenic ncALC220 region to reduce exoprotein release in MH96 when complemented. This reduction was not observed through complementation of the YeRER intergenic region devoid of the ncALC220 region (Fig. S7A). This data revealed the ncALC220 region as a key component of a complex regulatory network. Based on this, we can speculate that the ncALC220 may inhibit transcription or translation of ALC or RoeA (48, 49). *Trans* complementation of p184INT, p1845'*hoIA*, p184INT(K18), and p184ncALC220 in Δ ALC did not restore exoprotein release in Δ ALC but did reduce the proportion of elongated cells, with cell sizes similar to those observed for MH96 (Fig. S3). Based on these findings, we hypothesize that the complemented regions are diluting out an activator of RoeA, decreasing RoeA activity, which reduces the production of intracellular pre-exoprotein (Fig. 1B), and prevents cell elongation. The inability to complement within the intergenic region, in full or in part, to alter the cell morphology (Fig. S3) or exoprotein profile of the K18 strain, revealed that the missing nucleotides of the K18 3 bp deletion, 131 bp 5' of *roeA* are required for the expression of RoeA.

The absence of elongated cells in either the K18 or the *roeA* H12 mutants (Fig. S3) further supports the notion that RoeA is required to induce intracellular pre-exoprotein expression, which causes cell elongation. Of interest, the induction pAY-RoeA restored exoprotein release to K18 and H12 (similar to the *trans* complementation of p184INT_ALC in Δ ALC) but no Yen-Tc associated bands were observed. We assume this may relate to a combination of factors, such as the proximity of nc220 to its yet defined target, and/or most likely, the regulation of the Yen7- RoeA homologue.

The heterogeneity of the observed cell shapes and *HolA* expression reflect observations in other systems. In *S. marcescens* and *E. coli*, the expression of the exoproteins chitinase AB and colicin, respectively, caused cell elongation which was confined to a low proportion of cells (13, 50). In this respect, 0.6%, 6%, and 2% of *E. coli* cells that expressed colicin A, E2, and E7, respectively, were elongated (50). Using mKate fluorescence peptidase ChiX reporter, 1% of *S. marcescens* cells fluoresced which correlated to the co-expression of the ChiWXYZ lysis cluster and the ChiAB chitinases (13). The heterogeneous colicin expression is caused by bet-hedging, a risk spreading strategy in which stochastically occurring phenotypes of an isogenic population may adapt to changing environmental conditions (50, 51). Under *in vitro* conditions, exoprotein, including Yen-Tc, release is restricted to temperatures $\leq 25^{\circ}\text{C}$ (35), which reflects a

responsive switch rather than a stochastic switch (bet-hedging). In contrast to these *in vitro* findings, through the use of a YenA1 GFP reporter, elongated MH96 cells were observed *in vivo* in *G. mellonella* during early infection at 25°C but were absent at 37°C, where only a limited number of cells fluoresced (16, 18), indicating an additional layer of complexity in the regulatory system. Based on the results above, a model for the regulation of exoprotein production in *Y. entomophaga* is proposed in Fig. 8.

Based on the phylogenetic data, RoeA-like regulators identified in some bacteria of the Enterobacteriaceae and Yersiniaceae may also enable the release of other large macromolecular toxin-transporting assemblies, such as AFP/PVC complex of *P. chlororaphis*, through the activation of an ALC-like lysis cassette. Further research to define the role of RoeA and the ncRNA, ncALC220, in exoprotein regulation is required. The proposed model of *Y. entomophaga* MH96 mediated exoprotein release (Fig. 8) provides phenotypic evidence of the crucial role of a holin/endolysin-based system in the programmed release of proteins. It provides further support to the roles of these lysis systems as T10SS, as initially proposed by Palmer et al. (12) based on *in silico* analysis.

MATERIALS AND METHODS

Bacterial strains and culture conditions. Bacterial strains and plasmids used in this study are listed in Table S1 and Table S2, respectively. Bacteria were cultured in LB broth or on LB-agar at 25°C (*Y. entomophaga*) or 37°C (*E. coli*). For *E. coli* ST18, the culture medium was supplemented with 50 µg/mL 5-aminolevulinic acid. Unless stated, cultures were incubated with shaking at 250 rpm in a Ratek model OM11 orbital incubator. Antibiotic concentrations used were (µg/mL): *E. coli*, kanamycin (50), ampicillin (100); *Y. entomophaga*, kanamycin (100); spectinomycin (100), chloramphenicol (90), and tetracycline (15).

Molecular cloning. Standard DNA techniques were performed as described by Sambrook (52). Chromosomal DNA was isolated using PrepMan Ultra Sample Preparation Reagent (Thermo Fisher), and plasmid DNA was isolated using a High Pure Plasmid isolation kit (Roche). For amplification of genetic elements, Platinum *Taq* DNA polymerase (Invitrogen) was used according to manufacturer's guidelines. Amplicons were purified using High Pure PCR Product purification kit (Roche). Primers are listed in Table S5.

When required, PCR purified amplicons were ligated into pGEM-T Easy (Promega) following the manufacturer's instructions. The resultant construct sequences were validated using M13_F and M13_R universal primers, or in other cloned constructs using construct specific primers (Table S5). Sequencing was performed using Macrogen Sequencing Services (Macrogen Inc.). DNA was electroporated into *Y. entomophaga* and its derivatives using the method of Dower et al. (53).

Construction of ALC mutant. For the deletion of the ALC, 2 kb 5' and 2 kb 3' of the ALC operon were PCR amplified using the primer pairs MS82/83 and MS84/85, respectively. The primers MS83 and MS84 harbor a complementary sequence to the pKD4 encoded kanamycin cassette that was amplified using the primers MS01 and MS02. The resultant amplicons were then assembled using fusion-PCR. The purified fusion-PCR amplicon ΔALC was cloned into pGEM to form pGEM-ΔALC, from where it was cloned into the suicide vector pJP5608 using *SacI* restriction sites (pJP5608-ΔALC). *E. coli* ST18 was used to conjugate pJP5608-ΔALC into MH96. Trans-conjugants were selected on LB-agar with kanamycin and tested for loss of pJP5608 tetracycline resistance. The final mutant MH96-ΔALC was subjected to PCR and sequence was validated using the peripheral validation primers MS29 and MS30.

Construction of sfGFP reporter genes. PCR amplicons 5' HoIA (MS88/MS89) and 3' HoIA (MS90/MS91) from MH96, and the amplicon sfGFP from pBAD::sfGFP (Table S2), were cloned together using fusion-PCR with primers MS88 and MS91. The fusion was then cloned into pJP5608 using *XbaI* and *XmaI* restriction sites to form pJP5806-HoIAsfGFP. Fusion-PCR of 5' Rz1 (MS92/MS93), 3' Rz1 (MS94/MS95), and sfGFP was used to amplify amplicon Rz1-sfGFP, which was then cloned into pGEMT-easy. To enable selection, a spectinomycin cassette (MS96/MS97) was cloned into the Rz1-sfGFP *BamHI* restriction site, and the final amplicon Rz1-sfGFP-Spec cloned into pJP5608, *XbaI* and *XmaI* restriction sites to form pJP5608-Rz1sfGFP. Trans-conjugants were selected on LB-agar for loss of pJP5608 tetracycline resistance and for Rz1-sfGFP growth on spectinomycin. The final strains were PCR and sequence validated using the peripheral validation primers MS98/MS99 and MS98/MS30 (Table S5).

Construction of p184 trans complementation vectors. To construct the p184 vector series (Fig. 7), the various regions of the MH96 wild *YerER* region were PCR amplified using PCR primers (Table S5). The resultant PCR amplicons were cloned into pGEM Teasy, from where they were cloned into pACYC184 using the pGEMTeasy derived *EcoRI* restriction site. The K18 intergenic region was amplified (INT[K18]) from K18. Using GeneScript DNA of INT with a deletion of ncYLC220 (INTΔnvYLC220) and ncYLC220, truncations ncYLC80 and ncYLC110 flanked by *EcoRV* restriction were synthesized and used to clone into pACYC184 *EcoRV* to form the respective plasmids p184 INTΔnvYLC220, p184ncYLC80, and p184ncYLC110. The pACYC184 constructs were sequence validated with primer set MS/MS and transformed into MH96, K18, ΔYLC, and H4.

Protein visualization and characterization. Standard sodium dodecyl sulfate-polyacrylamide gel electrophoresis (SDS-PAGE) was performed as described (54). Proteins were visualized by silver staining according to Blum et al. (55).

LC-ESI-MS/MS. For LC-ESI-MS/MS, the appropriate band was excised from 0.1% (wt/vol) SDS polyacrylamide gel stained with Coomassie brilliant blue, and prepared for LC-ESI-MS/MS spectrometry. Each gel band was analyzed by mass spectrometry after de-staining, reduction with 0.1 M tris (2-carboxyethyl) phosphine (Fluka Chemie GmbH), alkylation with 20 μ L of 0.15 M iodoacetamide (Sigma), and digestion for 18 h with 1 μ g of TPCK-trypsin (Promega) in the presence of 10% acetonitrile (ACN). After digestion, the peptides were dried and resuspended in 50 μ L of 0.1% FA prior to injection on the mass spectrometer.

LC-ESI-MS/MS was performed on a nanoflow Ultimate 3000 UPLC (Dionex) coupled to maXis impact HD mass spectrometer equipped with a CaptiveSpray source (Bruker Daltonik). For each sample, 1 μ L of the sample was loaded on a C18 PepMap100 nano-Trap column (300 μ m ID \times 5 mm, 5- micron 100 \AA) at a flow rate of 3000 nL/min. The trap column was then switched in line with the analytical column ProntoSIL C18AQ (100 μ m ID \times 150 mm 3-micron 200 \AA). The reverse phase elution gradient was from 2% to 20% to 45% over 60 min, total 84 min at a flow rate of 600 nL/min. Solvent A was LCMS-grade water with 0.1% formic acid (FA); solvent B was LCMS-grade ACN with 0.1% FA.

The Q-TOF Impact HD (Bruker Daltonics) mass spectrometer was set up in a data-dependent automatic MS/MS mode where a full scan spectrum (50-2000 m/z , 2 Hz) followed by 10 MS/MS (350 to 1500 m/z , 1-20Hz) of the most intense ions with charge states 2 to 3 selected.

Genome sequencing of K18. Genomic DNA for genome sequencing was isolated using the ISOLATE II Genomic DNA Kit (Bioline). For identification of DNA alterations in strain K18, Illumina HiSeq 2500 System by Macrogen Sequencing Services was used. DNA sequences were trimmed using Trim_Galore (http://www.bioinformatics.babraham.ac.uk/projects/trim_galore/). Nucleotide differences were identified by alignment of Illumina reads against the MH96 genome sequence using the conda package for breseq version 0.33.0 with default parameters <http://barriklab.org/wiki/bin/view/Lab/ToolsBacterialGenomeResequencing> (56).

Bioinformatic analysis. DNA sequences were trimmed and aligned against the genome of strain MH96 (GenBank accession number [NZ_CP010029.1](https://ncbi.nlm.nih.gov/nucl/NZ_CP010029.1)) using the Map to Reference function of Geneious Prime (57). Protein sequences were assessed using Phyre2 (<http://www.sbg.bio.ic.ac.uk/phyre2/html/page.cgi?id=index>) and BLASTP (<https://blast.ncbi.nlm.nih.gov/Blast.cgi>) with default settings. For gene synteny, the highest BLASTP hits to the query protein were used to pull genome data from the respective organism, covering 10 kb over the homologous genes. Multiple nucleotide alignments and Neighbor-Joining tree were then performed using standard settings in Geneious 10.0.9.

Amino acid alignments were performed using Geneious 10.0.9 using ClustalW and BLOSUM Matrix with a Gap open cost of 10 and a Gap extension cost of 0.1. Amino acid alignments were visualized using GeneDoc 2.7.000 (58).

Cloning of ALC constructs and RoeA in pAY2-4, and their arabinose-based induction. Variations of the ALC operon were cloned into pAY2-4 NdeI and XhoI site. The PCR amplicon of *hoIA/pepB/rz* using primer pair MS101 and MS104 was cloned into pAY2-4 to form pAY-ALC Δ *rz1* (*hoIA*, *pepB*, and *rz*). Optimized amplicons of the lysis cassette were synthesized at GeneArt (Thermo Fisher Scientific) and designed to encode: (i) *hoIA*, *pepB*, *rz*, and *rz1* as non-overlapping ORFs (pAY-ALC-opt), while maintaining ribosomal binding sites (*rbS*) and amino acid identity; (ii) optimized regions encoding *hoIA*, *pepB*, and *rz* (pAY-ALC Δ *rz1*-opt); (iii) optimized region encoding *hoIA*, *rz*, and *rz1* (pAY-ALC Δ *pepB*-opt); and (iv) *hoIA*, *pepB*, and *rz1* (pAY-ALC Δ *rz*-opt), refer to Table S3 for synthesized nucleotide sequence. Cells harboring pAY-ALC Δ *rz1*, pAY-ALC-opt, pAY-ALC Δ *pepB*-opt, pAY-ALC Δ *rz*-opt, and pAY-ALC Δ *rz1*-opt were grown in LB (40%) broth at 25°C and 200 rpm until an OD₆₀₀ of 1 was reached. The cultures were induced with arabinose (0.2% final concentration), or the same volume of dH₂O was added as control and placed at ambient temperature \sim 22°C on a rotating platform at 40 rpm. The OD₆₀₀ was measured every 15 min until 3 h and at 24 hpi.

For construction of pAY-RoeA, the primers set MS65/MS66 were used to PCR amplify the amplicon RoeA, the purified product then cloned into pGEM T-easy, and sequence validated with M13F/R primer. Using NdeI and XhoI cloning sites, the RoeA amplicon was cloned into the analogous sites of pAY-2 to form pAY-RoeA. Prospective pAY-RoeA clones were sequence validated using the AY_F and AY_R primers. pAY-RoeA was then electroporated into K18 cells. For pAY-RoeA induction, 50-mL cultures were grown in 40% LB to which 0.02% arabinose was added. The cultures were incubated for 16 h at 25°C under 250 rpm shaking from where samples were centrifuged at 8,000 \times *g* for 5 min to collect cell pellets and culture supernatant to assess using SDS-PAGE.

Light and fluorescence microscopy. For light microscopy, 3 μ L of a MH96 cell culture at 16 hpi were observed under phase contrast. For Live/Dead staining the Syto9/PI stain (LIVE/DEAD BacLight kit; Invitrogen) was used at a 1:1 ratio and incubated for 5 min in a 1.5 mL UV-safe tube. Cells were observed under an Olympus BX50 light microscope at \times 400 magnification for both light and fluorescence microscopy. The SYTO9 stain was visualized using a FITC filter with excitation of 460/515 nm, and the PI stain using Texas Red 545/610 nm filter. Cell counts were measured using the software ImageJ 1.47v (59).

Live-cell imaging. All cultures were grown in 100% LB broth (200 μ g/mL ampicillin) until OD = 1. For live-cell imaging, 10 μ L of the culture were induced with 0.6% arabinose and immediately pipetted onto agarose covered glass slides, and assessed by light microscopy within the first minute post induction. Agarose pads were used to eliminate cell movement during the imaging process. Live-cell imaging was undertaken using the LSM710 microscope operated with Axiovision System (Carl Zeiss).

RNA isolation. RNA isolation was performed using the RNA minikit (Qiagen), the corresponding RNAProtect Bacteria Reagent (Qiagen), and RNase-Free DNase Set Kits (Qiagen).

Three culture flasks per strain (H12 and MH96) were incubated to reach \log_{10} CFU mL⁻¹ of 9.5. From each culture flask, 1 mL of sample culture was immediately transferred into 2 mL RNA to protect bacteria (Qiagen) and vortexed. After 5 min incubation at 25°C, the samples were pelleted at 5,000 × *g* for 10 min. The supernatant was decanted, and pellets left to air dry at 37°C before freezing at -20°C.

RNA was isolated using the RNA minikit (Qiagen) following the manufacturer's instructions. Following the on-column DNA digest with RNase-free DNase, a second, off-column DNA digest was performed. To 40 μL RNA, RDD buffer (40 μL) and DNase stock I (2.5 μL) was added, and the volume adjusted to 100 μL with DNA-free water. After 10 min incubation time at 25°C, the RNA cleanup protocol (provided in the Qiagen RNA minikit) was followed. The RNA was eluted in 40 μL RNase-free water and isopropanol precipitated. The total volume was adjusted to 180 μL and 1% sodium acetate (3M) was added. Three times, ice cold 100% ethanol (600 μL) were added to the solution and vortexed. The microcentrifuge tube was then placed at -20°C overnight, after which the suspension was centrifuged (10,000 *g* for 30 min at 4°C) and supernatant discarded. The pellet was washed twice with ice cold 75% ethanol (500 μL) and pelleted at 10,000 × *g* for 5 min at 4°C, and the supernatant discarded. After the final wash step, the samples were pulse spun to remove residual ethanol by pipetting out residual supernatant. The pellets were air dried at 37°C for 30 min, and then resuspended in RNase-free water. The resuspended sample was quantified by nanodrop. Of the sample RNA, 6 mg/μL were placed into a reaction tube, and liquid was evaporated in a SpeedVac. RNAseq was quality controlled and performed by Macrogen.

RNAseq. The Illumina short reads were inspected for quality using FASTQC (<https://www.bioinformatics.babraham.ac.uk/projects/fastqc/>). Bases with low quality PHRED scores (PHRED < 15 using a sliding window of 4 bases) were trimmed (using TRIMMOMATIC) from the short-read library, as well as any Illumina adapter sequences. Paired reads that were longer than 36 bp were kept for further analysis. The *Y. entomophaga* MH96 genome (Aug2018.NCBI.gb) was converted from GenBank format to fasta format using a custom BIOPYTHON script prior to indexing. Gene annotations were converted to gff format using the BIOPERL program bp_genbank2gff3.pl (https://manpages.debian.org/testing/bioperl/bp_genbank2gff3.1p.en.html). The genome fasta file was indexed, and the short-read libraries aligned to the reference genome using HISAT2 with the default parameters. STRINGTIE was used for novel transcript assemblies, and BALLGOWN calculated the transcript count matrix for each sample.

The transcript count matrix was read into R, and differential gene expression calculated using the DESeq2 package (60). Genes were considered differentially expressed when the adjusted *P* value (p_{adj}) was less than 0.05. For analysis purposes, differentially expressed genes of a log2Fold change < -1 and > 1 were considered of interest, and further assessed.

β-gal assays. For β-gal assays, an over-night culture was used to inoculate (1%) 50-mL LB flasks that were incubated at either 25 or 37°C with 200 rpm shaking. For the assay, at each time point, 2 × 200 μL of each culture were collected into a sterile 96-well plate (F-bottom) (Greiner Bio-One Cellstar) and then frozen at -80°C. Using a 96-well microplate reader SPECTROstarNano (BMG Labtech) and the MARS Data Analysis software (BMG Labtech), the rate of β-gal production was measured at OD₄₂₀ following the methods of Schaefer et al. (61, 62) with a custom β-gal mix: 60 mM Na₂HPO₄, 40 mM NaH₂PO₄, 10 mM KCl, 1mM MgSO₄, 1.8 μL mL⁻¹ β-mercaptoethanol, 0.2 mg mL⁻¹ Lysozyme from chicken egg (Sigma), 1:150 diluted Bacterial Protein Extraction Reagent (Thermo Fisher); and 1 mg mL⁻¹ of 2-nitrophenyl-β-galactopyranoside (Sigma). To control for temperature-dependent differences in the MH96 calibration curves measured at OD₆₀₀ for 25 and 37°C, an appropriate calibrating factor was applied to the Miller Unit Equivalent calculation.

Data availability. Sequencing data was deposited in the NCBI databank with the BioProject PRJNA892653 with BioSample association numbers SAMN31393954, SAMN31393955, SAMN31393956 for MH96 transcriptome reads (MH1, MH2, MH3), and SAMN31393957, SAMN31393958, SAMN31393959 for H12 (*roeA* mutant) reads (RoeA1, RoeA2, RoeA3).

SUPPLEMENTAL MATERIAL

Supplemental material is available online only.

SUPPLEMENTAL FILE 1, XLSX file, 0.2 MB.

SUPPLEMENTAL FILE 2, PDF file, 1.5 MB.

SUPPLEMENTAL FILE 3, MP4 file, 6.2 MB.

SUPPLEMENTAL FILE 4, MP4 file, 4.4 MB.

ACKNOWLEDGMENTS

We thank Ruy Jauregu for bioinformatic Hiseq assessment of the K18 strain, and Sandra Jones and Ancy Thomas for LC-ESI-MSMS of the MH96 supernatant. We also want to thank Martin Pilhofer and Miki Feldmüller from the Institute of Molecular Biology & Biophysics, Eidgenössische Technische Hochschule, Zürich for the providing tools and critical analysis of live-cell and fluorescent microscopy imaging.

This work was supported by the Ministry of Business, Innovation and Employment, New Zealand (Next Generation Bio-pesticides, grant number C10X1310), Callaghan Innovation R&D fellowship grant, and support from the Bio-Protection Research Centre.

REFERENCES

- Christensen JE, Pacheco SA, Konkell ME. 2009. Identification of a *Campylobacter jejuni*-secreted protein required for maximal invasion of host cells. *Mol Microbiol* 73:650–662. <https://doi.org/10.1111/j.1365-2958.2009.06797.x>.
- Haurat MF, Aduse-Opoku J, Rangarajan M, Dorobantu L, Gray MR, Curtis MA, Feldman MF. 2011. Selective sorting of cargo proteins into bacterial membrane vesicles. *J Biol Chem* 286:1269–1276. <https://doi.org/10.1074/jbc.M110.185744>.
- Maffei B, Francetic O, Subtil A. 2017. Tracking proteins secreted by bacteria: what's in the toolbox? *Front Cell Infect Microbiol* 7:221. <https://doi.org/10.3389/fcimb.2017.00221>.
- Green ER, Mecsas J. 2016. Bacterial secretion systems: an overview. *Microbiol Spectr* 4:10. <https://doi.org/10.1128/microbiolspec.VMBF-0012-2015>.
- Li N, Zhu Y, LaFrentz BR, Evenhuis JP, Hunnicutt DW, Conrad RA, Barbier P, Gullstrand CW, Roets JE, Powers JL, Kulkarni SS, Erbes DH, Garcia JC, Nie P, McBride MJ. 2017. The Type IX secretion system is required for virulence of the fish pathogen *Flavobacterium columnare*. *Appl Environ Microbiol* 83:e01769-17. <https://doi.org/10.1128/AEM.01769-17>.
- Toyofuku M, Carcamo-Oyarce G, Yamamoto T, Eisenstein F, Hsiao CC, Kurosawa M, Gademann K, Pilhofer M, Nomura N, Eberl L. 2017. Pro-phage-triggered membrane vesicle formation through peptidoglycan damage in *Bacillus subtilis*. *Nat Commun* 8:481. <https://doi.org/10.1038/s41467-017-00492-w>.
- Turnbull L, Toyofuku M, Hynen AL, Kurosawa M, Pessi G, Petty NK, Osvath SR, Carcamo-Oyarce G, Gloag ES, Shimon R, Omasits U, Ito S, Yap X, Monahan LG, Cavaliere R, Ahrens CH, Charles IG, Nomura N, Eberl L, Whitchurch CB. 2016. Explosive cell lysis as a mechanism for the biogenesis of bacterial membrane vesicles and biofilms. *Nat Commun* 7:11220. <https://doi.org/10.1038/ncomms11220>.
- Vacheron J, Heiman CM, Keel C. 2021. Live cell dynamics of production, explosive release and killing activity of phage tail-like weapons for *Pseudomonas* kin exclusion. *Commun Biol* 4:87. <https://doi.org/10.1038/s42003-020-01581-1>.
- Beveridge TJ. 1999. Structures of Gram-negative cell walls and their derived membrane vesicles. *J Bacteriol* 181:4725–4733. <https://doi.org/10.1128/JB.181.16.4725-4733.1999>.
- Kulp A, Kuehn MJ. 2010. Biological functions and biogenesis of secreted bacterial outer membrane vesicles. *Annu Rev Microbiol* 64:163–184. <https://doi.org/10.1146/annurev.micro.091208.073413>.
- Roier S, Zingl FG, Cakar F, Durakovic S, Kohl P, Eichmann TO, Klug L, Gadermaier B, Weinzerl K, Prassl R, Lass A, Daum G, Reidl J, Feldman MF, Schild S. 2016. A novel mechanism for the biogenesis of outer membrane vesicles in Gram-negative bacteria. *Nat Commun* 7:10515. <https://doi.org/10.1038/ncomms10515>.
- Palmer T, Finney AJ, Saha CK, Atkinson GC, Sargent F. 2021. A holin/peptidoglycan hydrolase-dependent protein secretion system. *Mol Microbiol* 115:345–355. <https://doi.org/10.1111/mmi.14599>.
- Hamilton JJ, Marlow VL, Owen RA, Costa MA, Guo M, Buchanan G, Chandra G, Trost M, Coulthurst SJ, Palmer T, Stanley-Wall NR, Sargent F. 2014. A holin and an endopeptidase are essential for chitinolytic protein secretion in *Serratia marcescens*. *J Cell Biol* 207:615–626. <https://doi.org/10.1083/jcb.201404127>.
- Hurst MR, Beattie A, Altermann E, Moraga RM, Harper LA, Calder J, Laugraud A. 2016. The draft genome sequence of the *Yersinia entomophaga* entomopathogenic type strain MH96^T. *Toxins* 8:143. <https://doi.org/10.3390/toxins8050143>.
- Paulson AR, O'Callaghan M, Zhang XX, Rainey PB, Hurst MRH. 2021. *In vivo* transcriptome analysis provides insights into host-dependent expression of virulence factors by *Yersinia entomophaga* MH96, during infection of *Galleria mellonella*. *G3 (Bethesda)* 11. <https://doi.org/10.1093/g3journal/jkaa024>.
- Hurst MRH, Jones SA, Binglin T, Harper LA, Jackson TA, Glare TR. 2011. The main virulence determinant of *Yersinia entomophaga* MH96 is a broad-host-range toxin complex active against insects. *J Bacteriol* 193:1966–1980. <https://doi.org/10.1128/JB.01044-10>.
- Schoof M, O'Callaghan M, Sheen CR, Glare TR, Hurst MRH. 2022. Identification of genes involved in exoprotein release using a high-throughput exoproteome screening assay in *Yersinia entomophaga*. *PLoS One* 17: e0263019. <https://doi.org/10.1371/journal.pone.0263019>.
- Hurst MR, Beattie AK, Jones SA, Hsu PC, Calder J, van Koten C. 2015. Temperature-dependent *Galleria mellonella* mortality as a result of *Yersinia entomophaga* infection. *Appl Environ Microbiol* 81:6404–6414. <https://doi.org/10.1128/AEM.00790-15>.
- Makino K, Shinagawa H, Amemura M, Kimura S, Nakata A, Ishihama A. 1988. Regulation of the phosphate regulon of *Escherichia coli*. Activation of pstS transcription by PhoB protein *in vitro*. *J Mol Biol* 203:85–95. [https://doi.org/10.1016/0022-2836\(88\)90093-9](https://doi.org/10.1016/0022-2836(88)90093-9).
- Okamura H, Hanaoka S, Nagadoi A, Makino K, Nishimura Y. 2000. Structural comparison of the PhoB and OmpR DNA-binding/transactivation domains and the arrangement of PhoB molecules on the phosphate box. *J Mol Biol* 295:1225–1236. <https://doi.org/10.1006/jmbi.1999.3379>.
- Bontemps-Gallo S, Fernandez M, Dewitte A, Raphael E, Gherardini FC, Elizabeth P, Koch L, Biot F, Reboul A, Sebbane F. 2019. Nutrient depletion may trigger the *Yersinia pestis* OmpR-EnvZ regulatory system to promote flea-borne plague transmission. *Mol Microbiol* 112:1471–1482. <https://doi.org/10.1111/mmi.14372>.
- Chakraborty S, Kenney LJ. 2018. A new role of OmpR in acid and osmotic stress in *Salmonella* and *E. coli*. *Front Microbiol* 9:2656. <https://doi.org/10.3389/fmicb.2018.02656>.
- Groisman EA. 2016. Feedback control of two-component regulatory systems. *Annu Rev Microbiol* 70:103–124. <https://doi.org/10.1146/annurev-micro-022115-095331>.
- Lubin EA, Henry JT, Fiebig A, Crosson S, Laub MT. 2016. Identification of the PhoB regulon and role of PhoU in the phosphate starvation response of *Caulobacter crescentus*. *J Bacteriol* 198:187–200. <https://doi.org/10.1128/JB.00658-15>.
- Starke M, Fuchs TM. 2014. YmoA negatively controls the expression of insecticidal genes in *Yersinia enterocolitica*. *Mol Microbiol* 92:287–301. <https://doi.org/10.1111/mmi.12554>.
- Starke M, Richter M, Fuchs TM. 2013. The insecticidal toxin genes of *Yersinia enterocolitica* are activated by the thermolabile LTTR-like regulator TcaR2 at low temperatures. *Mol Microbiol* 89:596–611. <https://doi.org/10.1111/mmi.12296>.
- Blasi U, Fraisl P, Chang CY, Zhang N, Young R. 1999. The C-terminal sequence of the lambda holin constitutes a cytoplasmic regulatory domain. *J Bacteriol* 181:2922–2929. <https://doi.org/10.1128/JB.181.9.2922-2929.1999>.
- Vukov N, Scherer S, Hibbert E, Loessner MJ. 2000. Functional analysis of heterologous holin proteins in a lambdaDeltaS genetic background. *FEMS Microbiol Lett* 184:179–186. <https://doi.org/10.1111/j.1574-6968.2000.tb09011.x>.
- Briers Y, Peeters LM, Volckaert G, Lavigne R. 2011. The lysis cassette of bacteriophage varphiKIMV encodes a signal-arrest-release endolysin and a pinholin. *Bacteriophage* 1:25–30. <https://doi.org/10.4161/bact.1.1.14868>.
- Rajaure M, Berry J, Kongari R, Cahill J, Young R. 2015. Membrane fusion during phage lysis. *Proc Natl Acad Sci U S A* 112:5497–5502. <https://doi.org/10.1073/pnas.1420588112>.
- Buchner S, Schlundt A, Lassak J, Sattler M, Jung K. 2015. Structural and functional analysis of the signal-transducing linker in the pH-responsive one-component system CadC of *Escherichia coli*. *J Mol Biol* 427:2548–2561. <https://doi.org/10.1016/j.jmb.2015.05.001>.
- Martinez-Hackert E, Stock AM. 1997. The DNA-binding domain of OmpR: crystal structures of a winged helix transcription factor. *Structure* 5: 109–124. [https://doi.org/10.1016/s0969-2126\(97\)00170-6](https://doi.org/10.1016/s0969-2126(97)00170-6).
- Blanco AG, Sola M, Gomis-Ruth FX, Coll M. 2002. Tandem DNA recognition by PhoB, a two-component signal transduction transcriptional activator. *Structure* 10:701–713. [https://doi.org/10.1016/s0969-2126\(02\)00761-x](https://doi.org/10.1016/s0969-2126(02)00761-x).
- Schlundt A, Buchner S, Janowski R, Heydenreich T, Heermann R, Lassak J, Geerlof A, Stehle R, Niessing D, Jung K, Sattler M. 2017. Structure-function analysis of the DNA-binding domain of a transmembrane transcriptional activator. *Sci Rep* 7:1051. <https://doi.org/10.1038/s41598-017-01031-9>.
- Hurst MRH, Becher SA, Young SD, Nelson TL, Glare TR. 2010. *Yersinia entomophaga* sp. nov. isolated from the New Zealand grass grub *Costelytra zealandica*. *Int J Syst Evol Microbiol* 61:844–849. <https://doi.org/10.1099/ijs.0.024406-0>.
- Lang B, Blot N, Bouffartigues E, Buckle M, Geertz M, Gualerzi CO, Mavathur R, Muskhelishvili G, Pon CL, Rimsky S, Stella S, Babu MM, Travers A. 2007. High-affinity DNA binding sites for H-NS provide a molecular basis for selective silencing within proteobacterial genomes. *Nucleic Acids Res* 35:6330–6337. <https://doi.org/10.1093/nar/gkm712>.
- Springer K, Sanger PA, Felsl A, Fuchs TM. 2021. Lon protease- and temperature-dependent activity of a lysis cassette located in the insecticidal island of *Yersinia enterocolitica*. *J Bacteriol* 203:e00616-20. <https://doi.org/10.1128/JB.00616-20>.
- Rennell D, Poteete AR. 1985. Phage P22 lysis genes: nucleotide sequences and functional relationships with T4 and lambda genes. *Virology* 143: 280–289. [https://doi.org/10.1016/0042-6822\(85\)90115-1](https://doi.org/10.1016/0042-6822(85)90115-1).

39. Young JP, Mathews CK. 1992. Interactions between T4 phage-coded deoxycytidylate hydroxymethylase and thymidylate synthase as revealed with an anti-idiotypic antibody. *J Biol Chem* 267:10786–10790. [https://doi.org/10.1016/S0021-9258\(19\)50087-4](https://doi.org/10.1016/S0021-9258(19)50087-4).
40. Kamilla S, Jain V. 2016. Mycobacteriophage D29 holin C-terminal region functionally assists in holin aggregation and bacterial cell death. *FEBS J* 283:173–190. <https://doi.org/10.1111/febs.13565>.
41. White R, Chiba S, Pang T, Dewey JS, Savva CG, Holzenburg A, Pogliano K, Young R. 2011. Holin triggering in real time. *Proc Natl Acad Sci U S A* 108:798–803. <https://doi.org/10.1073/pnas.1011921108>.
42. Berry J, Rajaure M, Pang T, Young R. 2012. The spanin complex is essential for lambda lysis. *J Bacteriol* 194:5667–5674. <https://doi.org/10.1128/JB.01245-12>.
43. Cahill J, Young R. 2019. Phage lysis: multiple genes for multiple barriers. *Adv Virus Res* 103:33–70. <https://doi.org/10.1016/bs.aivir.2018.09.003>.
44. Bervoets I, Charlier D. 2019. Diversity, versatility and complexity of bacterial gene regulation mechanisms: opportunities and drawbacks for applications in synthetic biology. *FEMS Microbiol Rev* 43:304–339. <https://doi.org/10.1093/femsre/fuz001>.
45. Krin E, Danchin A, Soutourina O. 2010. Decrypting the H-NS-dependent regulatory cascade of acid stress resistance in *Escherichia coli*. *BMC Microbiol* 10:273. <https://doi.org/10.1186/1471-2180-10-273>.
46. Ono S, Goldberg MD, Olsson T, Esposito D, Hinton JC, Ladbury JE. 2005. H-NS is a part of a thermally controlled mechanism for bacterial gene regulation. *Biochem J* 391:203–213. <https://doi.org/10.1042/BJ20050453>.
47. Picker MA, Wing HJ. 2016. H-NS, its family members and their regulation of virulence genes in *Shigella* species. *Genes* 7:112. <https://doi.org/10.3390/genes7120112>.
48. Reuther J, Schneider L, Iacovache I, Pircher A, Gharib WH, Zuber B, Polacek N. 2021. A small ribosome-associated ncRNA globally inhibits translation by restricting ribosome dynamics. *RNA Biol* 18:2617–2632. <https://doi.org/10.1080/15476286.2021.1935573>.
49. Wyss L, Waser M, Gebetsberger J, Zywicki M, Polacek N. 2018. mRNA-specific translation regulation by a ribosome-associated ncRNA in *Haloflex volcanii*. *Sci Rep* 8:12502. <https://doi.org/10.1038/s41598-018-30332-w>.
50. Bayramoglu B, Toubiana D, van Vliet S, Inglis RF, Shnerb N, Gillor O. 2017. Bet-hedging in bacteriocin producing *Escherichia coli* populations: the single cell perspective. *Sci Rep* 7:42068. <https://doi.org/10.1038/srep42068>.
51. Veening JW, Smits WK, Kuipers OP. 2008. Bistability, epigenetics, and bet-hedging in bacteria. *Annu Rev Microbiol* 62:193–210. <https://doi.org/10.1146/annurev.micro.62.081307.163002>.
52. Sambrook J, F E, Maniatis T. 1989. Molecular cloning, 2nd edition. Cold Spring Harbor Laboratory Press, Long Island, NY.
53. Dower WJ, Miller JF, Ragsdale CW. 1988. High efficiency transformation of *E. coli* by high voltage electroporation. *Nucleic Acids Res* 16:6127–6145. <https://doi.org/10.1093/nar/16.13.6127>.
54. Laemmli UK. 1970. Cleavage of structural proteins during the assembly of the head of bacteriophage T4. *Nature* 227:680–685. <https://doi.org/10.1038/227680a0>.
55. Blum H, Beier H, Gross HJ. 1987. Improved silver staining of plant proteins, RNA and DNA in polyacrylamide gels. *Electrophoresis* 8:93–99. <https://doi.org/10.1002/elps.1150080203>.
56. Deathage DE, Barrick JE. 2014. Identification of mutations in laboratory-evolved microbes from next-generation sequencing data using breseq. *Methods Mol Biol* 1151:165–188. https://doi.org/10.1007/978-1-4939-0554-6_12.
57. Kearse M, Moir R, Wilson A, Stones-Havas S, Cheung M, Sturrock S, Buxton S, Cooper A, Markowitz S, Duran C, Thierer T, Ashton B, Meintjes P, Drummond A. 2012. Geneious Basic: an integrated and extendable desktop software platform for the organization and analysis of sequence data. *Bioinformatics* 28:1647–1649. <https://doi.org/10.1093/bioinformatics/bts199>.
58. Caffrey DR, Dana PH, Mathur V, Ocano M, Hong EJ, Wang YE, Somaroo S, Caffrey BE, Potluri S, Huang ES. 2007. PFAAT version 2.0: a tool for editing, annotating, and analyzing multiple sequence alignments. *BMC Bioinformatics* 8:381. <https://doi.org/10.1186/1471-2105-8-381>.
59. Schneider CA, Rasband WS, Eliceiri KW. 2012. NIH Image to ImageJ: 25 years of image analysis. *Nat Methods* 9:671–675. <https://doi.org/10.1038/nmeth.2089>.
60. Love MI, Huber W, Anders S. 2014. Moderated estimation of fold change and dispersion for RNA-seq data with DESeq2. *Genome Biol* 15:550. <https://doi.org/10.1186/s13059-014-0550-8>.
61. Schaefer J, Jovanovic G, Kotta-Loizou I, Buck M. 2016. A data comparison between a traditional and the single-step beta-galactosidase assay. *Data Brief* 8:350–352. <https://doi.org/10.1016/j.dib.2016.05.063>.
62. Schaefer J, Jovanovic G, Kotta-Loizou I, Buck M. 2016. Single-step method for beta-galactosidase assays in *Escherichia coli* using a 96-well microplate reader. *Anal Biochem* 503:56–57. <https://doi.org/10.1016/j.ab.2016.03.017>.